

Thermophysical Features of Shallow Lunar Crust Demonstrated by Typical Copernican Craters Using CE-2 CELMS Data

Zhiguo Meng^{1,2}, Member, IEEE, Xiangyue Li, Shengbo Chen, Yongchun Zheng, Jiancheng Shi^{1,2}, Fellow, IEEE, Tianxing Wang^{1,2}, Member, IEEE, Yuanzhi Zhang, Member, IEEE, Jinsong Ping, and Yu Lu^{1,2}

Abstract—Chang’E lunar microwave sounder (CE-2 CELMS) data provide a potential way to understand the thermophysical features of the shallow lunar crust. In this study, four typical Copernican craters, including Copernicus, Aristarchus, Tycho, and Jackson, have been selected and their brightness temperature (T_B) performances are evaluated with the CE-2 CELMS data. The results are as follows. First, the hot T_B anomaly is reunderstood according to the T_B behaviors. The cause to the anomaly is still in doubt, and we rule out the previous explanations as rock abundance or topography. Second, the existence of the cold anomaly indicates the shallow lunar crust is likely much colder than what we knew. Third, the T_B performances indicate that the shallow lunar crust is likely homogeneous, and the materials here have very low ($\text{FeO} + \text{TiO}_2$) abundance and thermal inertia. Also, the difference of the T_B performances from the crater floors to far distance will provide a new constraint for the cratering formation study.

Index Terms—Chang’E lunar microwave sounder (CE-2 CELMS) data, microwave thermal emission, shallow lunar crust, thermophysical features, typical Copernican craters.

Manuscript received September 7, 2018; revised December 3, 2018; accepted December 27, 2018. Date of publication February 12, 2019; date of current version July 30, 2019. This work was supported in part by the National Key R&D Program of China under Grant 2018YFB0504700, in part by the opening fund of State Key Laboratory of Lunar and Planetary Sciences (Macau University of Science and Technology) under Macau FDCT Grant 119/2017/A3, in part by the National Natural Science Foundation of China under Grants 41371332, 41490633, and 41490634, in part by the Science and Technology Development Fund of Macau under Grant 0012/2018/A1, in part by the Program for JLU Science and Technology Innovative Research Team under Grant 2017TD-26, and in part by the Pioneer Science and Technology Special Training Program B (No. XDPB11-01-04) of Chinese Academy of Sciences. (Corresponding author: Zhiguo Meng.)

Z. Meng, X. Li, and S. Chen are with the College of Geoexploration Science and Technology, Jilin University, Changchun 130026, China, and also with State Key Laboratory of Lunar and Planetary Sciences, Macau University of Science and Technology, Macau (e-mail: menggz@jlu.edu.cn; xiangyue17@mails.jlu.edu.cn; chensb@jlu.edu.cn).

Y. Zheng, Y. Zhang, and J. Ping are with the Key Laboratory of Lunar and Deep-Space Exploration, Chinese Academy of Sciences, Beijing 100011, China (e-mail: zyc@bao.ac.cn; yzzhang309@163.com; jsping@bao.ac.cn).

J. Shi and T. Wang are with the State Key Laboratory of Remote Sensing Science, Institute of Remote Sensing and Digital Earth, Chinese Academy of Sciences, Beijing 100101, China (e-mail: shje@radi.ac.cn; wangtx@radi.ac.cn).

Y. Lu is with School of Geography and Ocean Science, Nanjing University, Nanjing, 210023, China, and also with Jiangsu Center for Collaborative Innovation in Geographical Information Resource Development and Application, Nanjing, 210023, China (e-mail: njluyu@qq.com).

Color versions of one or more of the figures in this paper are available online at <http://ieeexplore.ieee.org>.

Digital Object Identifier 10.1109/JSTARS.2019.2892361

TABLE I
POSITION AND SIZE OF TYPICAL COPERNICAN CRATERS [1]–[7]

Crater	Position	Diameter (km)	Depth (km)	Age (Ma)
Copernicus	9.6°N, 20.0°W	93	~6.0–7.0	~(800±15)
Tycho	43.3°S, 11.2°W	86	~7.0	~(109±4)
Aristarchus	23.7°N, 47.4°W	40	~3.7	~450
Jackson	22.4°N, 163.1°W	71	~6.0	

I. INTRODUCTION

COPERNICAN craters are the latest craters occurred on the Moon surface, which penetrated the shallow lunar crust about several kilometers decided by the sizes of the impact craters (see Table I) [1]–[7]. Therefore, the study on the thermal behaviors of the typical Copernican craters will give wonderful clues about the thermal state and the thermophysical features of the shallow lunar crust [8], [9].

Up to now, remotely-sensed observations are always the most important way to study the thermophysical features of the lunar regolith in the Copernican craters combined with the earth-based observation and samples at Apollo, Luna, and Surveyor programs [9]–[17]. Remote observations acquired the surface information at ultraviolet through microwave wavelengths. The visible observations at short wavelengths are good to estimate the composition and physical properties of the upper few millimeters of surfaces [18], [19]. Surface temperatures derived from thermal infrared (TIR) measurements are sensitive to the thermal conductivity of the surface layer to a depth about several centimeters for highly insulating dust [16], [20], [21]. Radar observations are highly sensitive to the rocks similar in size to the wavelength of measurements [10].

The brightness temperature (T_B) measurement in microwave range provides a fourth means of understanding the thermophysical properties of the lunar regolith in the Copernican craters [9], [11], [14], [22], [23]. The measurement is proved to be sensitive to the temperature and composition of the regolith layer to a depth about 10 to 20 times of the used wavelength [11], [15]. This provides a potential possibility to study the thermophysical features of the shallow lunar crust demonstrated by the Copernican craters.

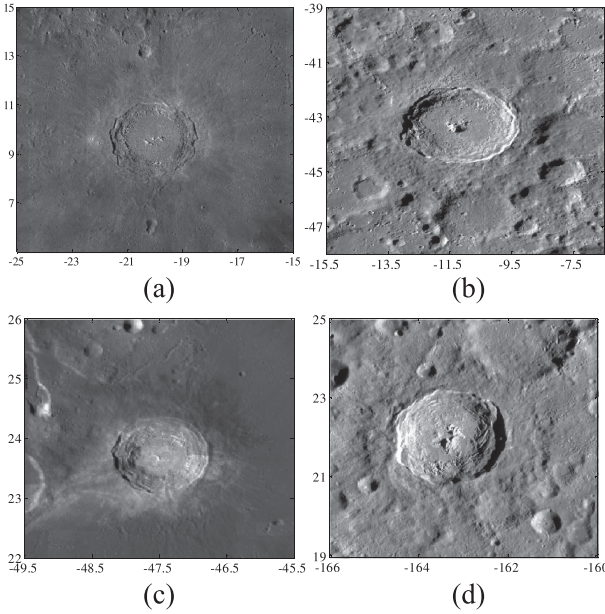


Fig. 1. WAC images of typical Copernican craters. The data were downloaded from <http://wms.lroc.asu.edu/lroc-thumbnails?camera=WAC&phase=SMD>.

This work employed data collected from the microwave sounder (CELMS) onboard Chang'E (CE)-1/2 lunar orbiters. Chan *et al.* [13] and Zheng *et al.* [9] firstly well studied the thermal behaviors of the fresh craters of Aristarchus and Tycho with the CE-1 CELMS data, which gives a different view about their performances compared with the TIR measurements. Combined with the theoretical model, Gong and Jin attributed the discovered hot T_B anomaly at noon in Tycho crater to the rock abundance (RA) [24]. But, based on the CE-2 CELMS data, Meng *et al.* thought the surface slope and its orientation as the important factors to the hot anomaly in Tycho crater [14]. Whereas, Meng *et al.* attributed the cold T_B anomaly near Mare Crisium to a special material with rather low ($\text{FeO}+\text{TiO}_2$) abundance (FTA) according to the T_B performances combined with the composition and RA results [25]. Thus, systematic studies of the T_B performances should be done to better understand the regolith thermophysical features and their geologic meanings in global scale.

In this study, the microwave thermal emission (MTE) features of three more Copernican craters, including Copernicus, Aristarchus, and Jackson (see Fig. 1), are introduced to further study the thermophysical features of the shallow lunar crust. Section II briefly introduces the process of the CELMS data. Section III analyzes the MTE features of four typical craters. The applications of the T_B maps to understand the thermophysical features of the shallow lunar crust are discussed in Section IV. Section V is the conclusions.

II. DATA PROCESSING

A. CELMS Instrument and Data Description

CE-2 lunar orbiter was launched successfully on 1 October, 2010, and finished its observations on 9 June, 2011. The orbit

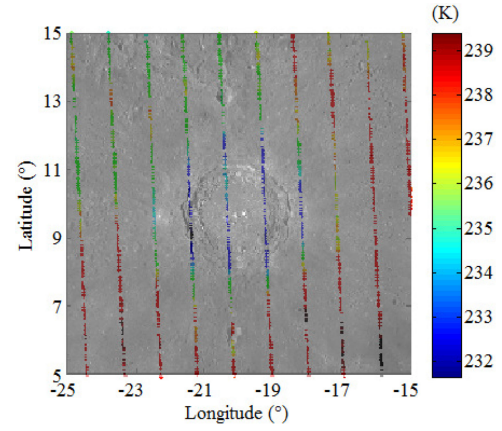


Fig. 2. Scatter map of the CELMS data at noon overlays on WAC image.

altitude is about 100 km, and this directly leads to an improvement in the spatial resolution for most of the instruments as compared with CE-1 orbiter [26].

The CELMS instrument is used to investigate MTE properties of the lunar regolith, which operates at 3.0, 7.8, 19.35, and 37.0 GHz. The observation angle is 0° [14], [29]. In this study, Level 2C swath data are used for lunar surface thermal properties investigation, which are the raw data processed after geometric correction and radiometric calibration [9], [27], [28]. Their archive format is Planetary Data System (PDS). As a single file, the 2C-level data contain a header and a table of measured data, which present the observation time, four-channel T_B s, solar incidence angle and azimuth angle, selenographic latitude and longitude, orbit altitude, and data quality state [9], [30].

According to the prelaunch calibration experiments, the radiometric accuracy is better than 0.5 K that depends on temperature and frequency. By comparing the observed T_B s at the Apollo 14, 15, and 17 landing sites, the estimated radiometric uncertainty is about 0.16 K for 3.0 and 7.8 GHz, 0.12 K for 19.35 GHz, and 0.14 K for 37.0 GHz [27], [28].

The nominal spatial resolution is 15 km for channels 7.8, 19.35, and 37.0 GHz, and is 25 km for 3.0 GHz [27], [28]. After overlying the obtained CELMS data on the lunar surface (see Fig. 2), 1° spatial resolution along the lines of constant latitude and very high spatial resolution along the longitude are clearly presented.

B. T_B Maps Construction

CELMS data processing has been thoroughly described by Chan *et al.* [13], Zheng *et al.* [9], and Meng *et al.* [14], [25], [29], [31]. The same data processing method is adopted in this study.

During the 8-month observation period, CE-2 CELMS obtained 2369 tracks of swath data that covered the Moon uniformly for about 15 times. However, the observation is randomly distributed at any time during the mission. Thus, in any given hour, the CELMS data are not enough to cover the whole Moon surface. To eliminate the influence of observation time, or surface temperature, on the final images, the hour angle is first

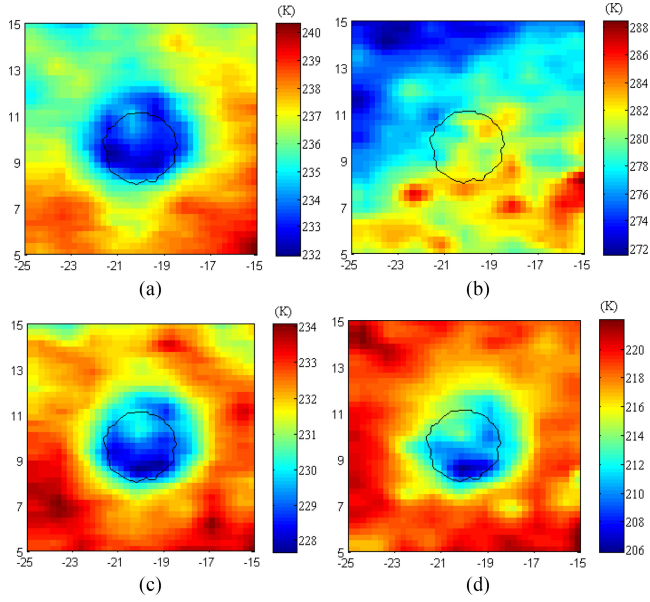


Fig. 3. T_B maps of Copernicus crater.

introduced to select the CELMS data with the similar surface conditions [14], [25], [29], [31].

For the deficiency of the original data, the observation time is selected at 12 and 0 O'clock for Copernicus crater, at 13 and 1 O'clock for Tycho crater, and at 12 and 1 O'clock for Aristarchus and Jackson craters, which are used to represent T_B at lunar noon and midnight, respectively. The temperature at noon is approximately highest and that is considerably low at midnight, which are the most appropriate times to study the MTE features of the lunar regolith in these craters [32], [33].

Additionally, the spatial resolution of the CELMS data is about 1° spatial resolution along the lines of constant latitude, while it is very high spatial resolution along the lines of constant longitude. As the variation of the T_B along latitude is low, the linear interpolation method is suitable under these conditions to improve the spatial resolution [14], [29]. Thereafter, the T_B maps were generated with a spatial resolution of $0.25^\circ \times 0.25^\circ$ (see Figs. 3–6), where the horizontal axis is the longitude, the vertical axis is the latitude, and the unit is degree.

Until recently, the T_B maps of the whole Moon were available by Zheng *et al.* [9], Chan *et al.* [13], and Wang *et al.* [27] using CE-1 CELMS data and Cai and Lan [26] using CE-2 CELMS data. Our T_B maps agree well with the previous results in values and spatial distributions. This implies the rationality of the generated T_B maps.

III. RESULTS

Copernican age began 0.8 billion years ago [1], [3]. The sizes of selected craters are large enough to identify the MTE features in the crater floor, rim, and their vicinity. Also, the T_B s at 3.0 and 37.0 GHz are two extreme phases in penetration depth, which are employed in this study. Additionally, to better understand the T_B performances, the rims of the craters are drawn and overlaid on Figs. 3–6, respectively.

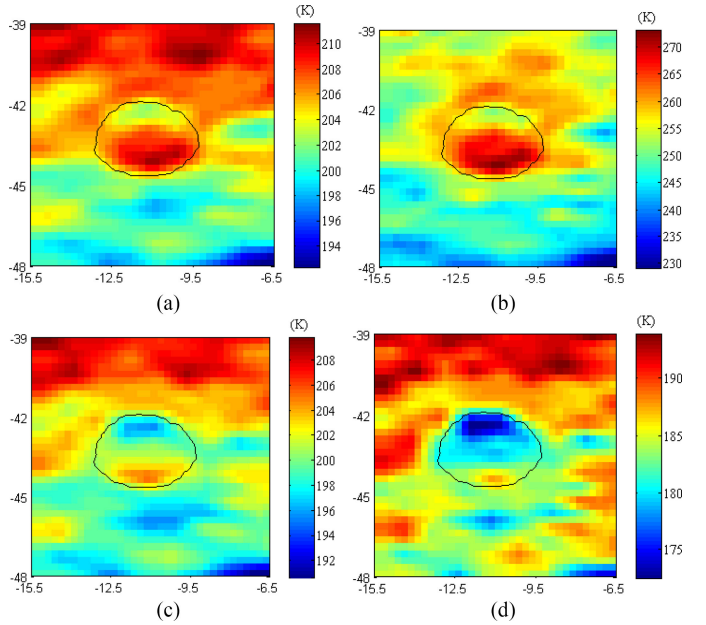


Fig. 4. T_B maps of Tycho crater.

A. Copernicus Crater

Copernicus crater (9.6° N, 20.0° W, 800 ± 15 Ma) is 93 km in diameter. The crater is in highlands and it is surrounded by Mare Insularum and Mare Imbrium [see Fig. 1(a)]. Earth-based spectroscopic measurements detected an olivine-bearing lithology in the central peaks [34], [35]. Impact melt deposits are extensively present in various parts of the crater [36]. Recently, proposed east–west differences and identification of Mg-spinel have expanded this diversity [37], [38].

Fig. 3 is the generated T_B maps at 12 (noon) and 0 O'clock (midnight). At noon, Fig. 3 indicates a rather low T_B distribution in the crater floor except that of 37.0 GHz. Especially, the T_B at 3.0 GHz is nearly evenly lower in the floor than its vicinity except a small patch in the middle of the northern part. But, the T_B at 37.0 GHz does not clearly present the crater, which agrees well with the proposed east–west differences by Arai *et al.* [38]. At midnight, the T_B clearly indicates that the crater floor is still much cooler than its vicinity. However, the distribution of the T_B is still not even in the crater floor. The T_B in most areas of the crater floor is rather low at 3.0 GHz, while only one quarter of the floor in the southwest gives low T_B at 37.0 GHz.

What is more, the shape of the region with relatively lower T_B is largely shown as a circle at 3.0 GHz whether at noon or midnight, while it is absolutely not a circle at 37.0 GHz.

What astonishes us is that the area of the region with low T_B is apparently beyond the crater range. Considering the strong impact of the topography on the observed T_B [33], [39], it is difficult to interpret the phenomenon, which is further studied in the following section.

B. Tycho Crater

Tycho crater (43.3° S, 11.2° W, 109 ± 4 Ma) is located in the southern highlands region on the lunar near side [see Fig. 1(b)],

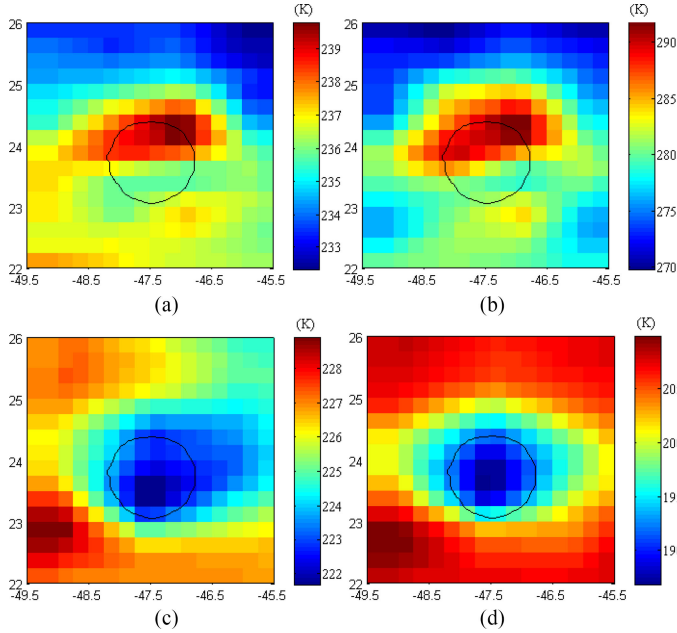


Fig. 5. T_B maps of Aristarchus crater.

which is 86 km in diameter. Tycho has an extensive ray system, a prominent central peak, and spectacular impact melt deposits [40]–[43]. The geomorphologic features of the Tycho crater have been thoroughly studied using LRO Camera (LROC) data and topography data [14]. TIR data were widely used to examine the thermal anomaly here [21], [44]. Also, the MTE features of the crater have been studied by Meng *et al.* using the CE-2 CELMS data [14].

Fig. 4 is the T_B maps at 13 (noon) and 1 O'clock (midnight), which indicates a special MTE feature in Tycho crater. The T_B in the northern outer wall and southern inner wall is fairly high whether at noon or midnight, while it is rather low in the northern part of the crater rim and floor and the southern outer wall. This agrees well with the observation by Salisbury and Hunt [45] and Meng *et al.* [14]. Moreover, the areas of the regions with high or low T_B values change greatly with frequency.

Moreover, the shape of the crater is largely well preserved at noon. But at midnight, the difference between the middle part of the crater floor and southern part of the highlands is not clear.

C. Aristarchus Crater

Aristarchus crater (23.7°N , 47.4°W , 450 Ma), 40 km in diameter, is a prominent Copernican crater in the western nearside of the Moon [see Fig. 1(c)]. The crater was formed at the contact between Procellarum basalts and an uplifted block of lunar crust, Aristarchus Plateau [46]. Materials in the crater are rich in feldspar-like anorthite [46]–[48]. Elsewhere on the crater wall the deposits were interpreted to be dominated by noritic compositions typical of the upper crust [46].

Fig. 5 shows a similar T_B performance as that in Tycho crater at noon, where the T_B in the southern outer wall and northern inner wall is fairly high, which is orientating to the solar illumination; and it is rather low in the southern part of the crater floor

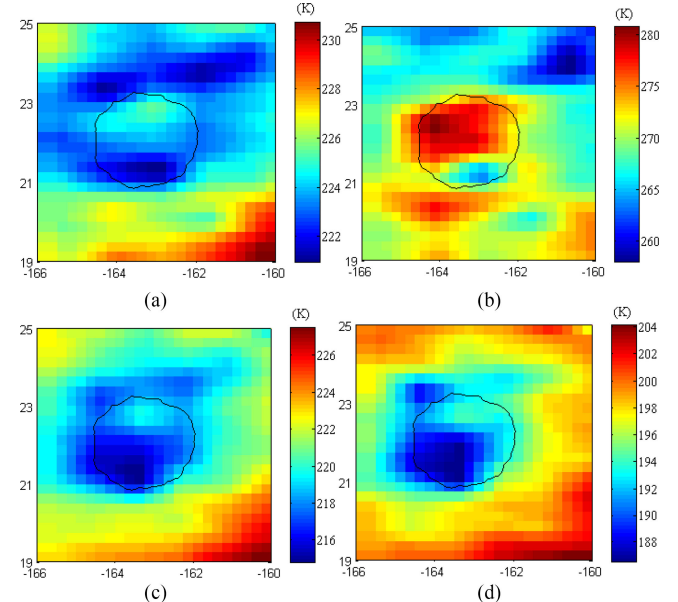


Fig. 6. T_B maps of Jackson crater.

and the northern outer wall, which is opposite to the solar illumination. Interestingly, at midnight, the T_B performance is similar to that in Copernicus crater, where the low T_B is distributed over the entire crater floor.

Moreover, the area of the regions with relatively higher T_B in the northern wall is increasing with the frequency at noon, and it disappeared at midnight. But the area of the regions with relatively lower T_B in the crater floor is apparently decreasing with frequency at midnight. The shape of the crater is not well preserved except at 37.0 GHz at midnight.

D. Jackson Crater

Jackson Crater (22.4°N , 163.1°W), 71 km in diameter, is located on east of Mare Moscovense and north of the South Pole Aitken basin [see Fig. 1(d)]. The crater has a spectacular ray system, well-formed terraces, and a cluster of central peaks. It is located in the highland terrane, suggesting its principal geologic setting to be feldspathic in nature [49]. The crater diameter indicates an excavation depth of about 6 km [4].

Fig. 6 obviously indicates a different T_B performance from other three craters. At noon, the low T_B shows a ring structure with the relatively higher T_B values in the northeastern part of the crater at 3.0 GHz and the range is apparently beyond the crater, while the ring structure is disappeared at 37.0 GHz. Additionally, the highest T_B occurs in the northwest part of the crater. At midnight, the low T_B behavior in and around the crater is largely similar to that at 3.0 GHz at noon, and the low T_B distributions at 37.0 GHz are largely limited in the western part of the crater.

Moreover, the shape of low T_B region is absolutely not a circle, and the range changes greatly with time and frequency, indicating special thermophysical features of the lunar regolith in this crater.

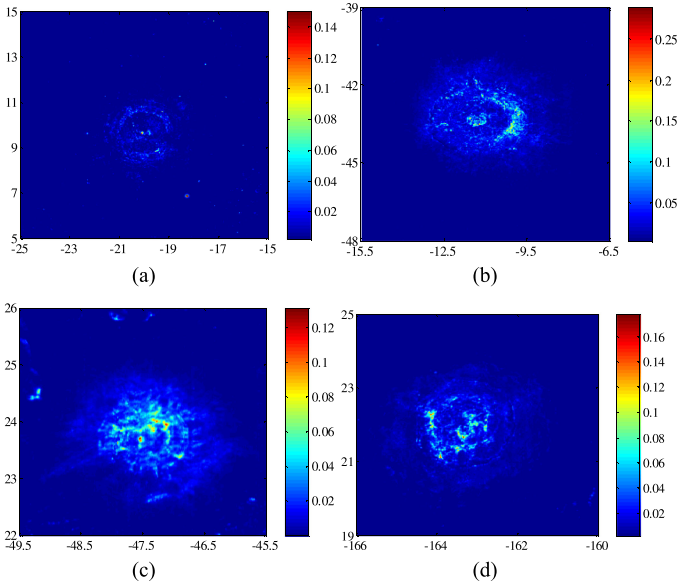


Fig. 7. RA maps of typical Copernican craters (100%).

IV. DISCUSSIONS

The T_B performances in typical Copernican craters bring some valuable information about the shallow lunar crust.

A. Hot T_B Anomaly

Hot T_B anomaly is obviously presented in the southern inner wall of Tycho crater and northern inner walls of Aristarchus and Jackson craters at noon. At midnight, cold T_B anomaly apparently exists in all four crater floors. Similar cold and hot anomalies have ever been observed with the ground-based TIR measurements [20], [21], [45], [50].

In previous studies, more attention have been paid to the hot T_B anomaly in Tycho crater. Williams *et al.* [51], Gong and Jin [24], and Hu *et al.* [39] attributed the anomaly to the existence of abundant rocks and boulder distributions. Similar result was also obtained by Bandfield *et al.* [16]. But Salisbury and Hunt [45] and Meng *et al.* [14] thought that the hot anomaly is dominated by the surface slope and its orientation.

To better understand the relationship between the T_B performances and the rock abundance (RA), the RA derived with the Lunar Reconnaissance Orbiter (LRO) Diviner data is introduced in this study (see Fig. 7), which was downloaded from the Java Mission-planning and Analysis for Remote Sensing (JMARS) software. The reliability was verified by their comparison with the results reported by Bandfield *et al.* [16].

Apparently, Fig. 7 indicates a weak correlation between the RA and the T_B distributions. In Copernicus crater, the RA is almost evenly distributed around the crater rim, while the T_B maps give a rather complex distribution at noon. Even at midnight, the low T_B anomaly exists in the crater only, and no high T_B values can be related to the RA distribution. In Tycho crater, high RA values mainly occur in the eastern rim and the central part of the floor, but the hot anomaly is positioned in the southern rim of the crater. In Aristarchus crater, high RA val-

TABLE II
CORRELATION COEFFICIENTS BETWEEN T_B AND RA

Time	Noon		Midnight		
	Channel	3.0	37.0	3.0	37.0
Copernicus		-0.65	0.37	-0.71	-0.68
Tycho		0.69	0.79	-0.09	-0.63
Aristarchus		0.87	0.88	-0.68	-0.92
Jackson		0.35	0.78	-0.66	-0.70

ues occur in the northern crater rim, which coincides well with the performances of the hot T_B anomaly at noon. But the hot T_B anomaly is diminished at midnight. In Jackson crater, high RA values exist in the western rim and the central part of the crater, but the hot anomaly occurs in the northern rim at noon and northeast rim at midnight. Therefore, the RA is obviously not the direct cause for the hot anomaly in these regions.

Table II is the correlation coefficients between the T_B and RA. Again, Table II indicates a complex influence of the RA on the T_B . If we ruled out Copernicus crater, the RA plays a strong influence on the T_B . At this condition, the correlation coefficients are positive at noon, and they are negative at midnight, indicating that the influential mechanism of the RA on the T_B is different at the two observation times. Moreover, the coefficients at 37 GHz are higher than those at 3.0 GHz, indicating that the T_B at 37 GHz likely experiences more impact from the rock distributions. However, if the correlation coefficients in Copernicus are taken into account, the aforementioned regularities are absolutely wrong. Here, the coefficient at 3.0 GHz is negative at noon, and the coefficients at 37 GHz are not higher than those at 3.0 GHz. This again validates that the RA is obviously not the direct cause for the hot anomaly in these regions.

As mentioned before, the hot anomaly has even been attributed to the surface slope and its orientation [14], [45]. This is only applicable for the Tycho, Aristarchus, and Jackson craters at noon, but not for Copernicus crater. Moreover, at midnight, the hot anomaly only exists in Tycho crater, but not in other three craters. That is, the topography is also ruled out as the cause for the hot T_B anomaly.

Based on theoretical model, Sinton also attributed the hot T_B anomaly to the thick dust layer on the surface of Tycho crater [21]. However, similar T_B performances do not occur in other three craters. This means, to some extent, that there is not a thick dust layer on the surface of other three craters. Considering the similar cratering mechanism of these four craters and surface conditions, such conclusion should be severely treated.

Therefore, the causes to the hot T_B anomaly are still in doubt, which should be further studied with more sources of the data, and even the *in situ* measurements.

B. Cold T_B Anomaly and Its Geologic Significance

Cold T_B anomaly, or cold spot [17], [21], is always neglected in the current lunar study. Sinton mentioned the cold spot within

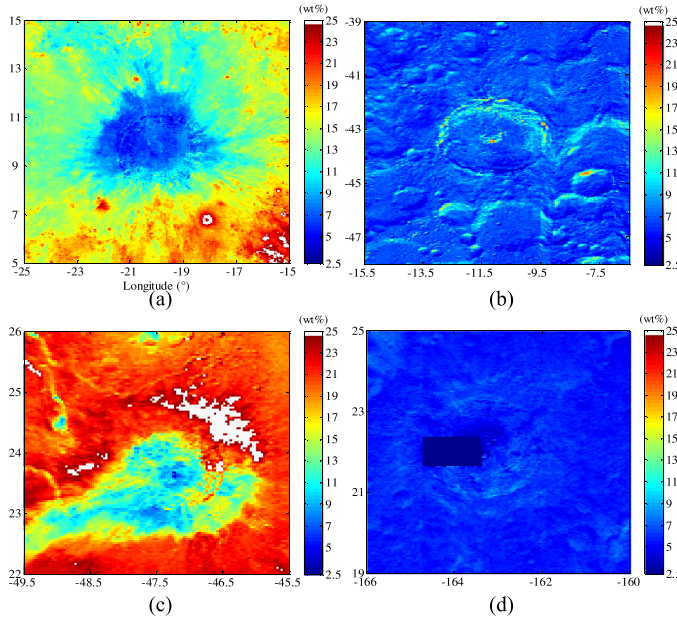


Fig. 8. FTA maps of typical Copernican craters.

Tycho crater, and he attributed it to the absence of the solar illumination [21]. Using Diviner data, Bandfield *et al.* attributed the cold anomaly to the absence of the rocks in the regolith in the upper 10–30 cm [17]. With the CE-1 CELMS data, Chan *et al.* [13] and Zheng *et al.* [9] preliminarily studied the MTE features of the cold anomalies over the Moon surface. According to the theoretical model and CE-1 CELMS data, Gong and Jin attributed the cold anomaly in Tycho crater at night to the high RA [24].

Interestingly, the low T_B anomaly is distributed in all four crater floors whether at noon or midnight. Therefore, the low T_B anomaly is weakly related to the topography.

Moreover, the T_B behavior is astonished in Copernicus crater at noon. At 3.0 GHz, the distribution of the cold anomaly is apparently beyond the crater range, especially in the northern inner crater wall orienting to the solar illumination. This not only opposes the impact of the topography on the cold T_B anomaly, but also rejects the topography impact on the hot T_B anomaly.

Additionally, the analysis in Section IV-A implies that the RA is likely not the cause for the cold T_B anomaly. Thus, more information should be introduced to better understand the cause for the cold anomaly. Based on the FTA inversed with Clementine UV-VIS data and the CELMS data, Meng *et al.* indicated a strong influence of the FTA on the T_B in the local scale [32]. Meng *et al.* also discovered that the cold anomaly near Mare Crisium is likely brought by a special material after comparing the T_B maps with the RA and FTA maps [25]. To better understand the mechanism bringing about the cold T_B anomaly, the FTA resulted from Clementine UV-VIS data is introduced (see Fig. 8), which was downloaded from the JMARS software. The reliability was verified by the comparison with the results reported by Lucey *et al.* [18].

Fig. 8 indicates a strong correlation between the FTA and the cold T_B anomaly. First, the regions with low T_B at midnight are

TABLE III
CORRELATION COEFFICIENTS BETWEEN T_B AND FTA

Time	Noon		Midnight		
	Channel	3.0	37.0	3.0	37.0
Copernicus		0.96	-0.16	0.91	0.81
Tycho		0.25	0.43	-0.33	-0.51
Aristarchus		-0.63	-0.57	0.30	0.68
Jackson		-0.84	0.44	-0.09	0.01

all located in the places with low FTA. Second, even at noon when the surface temperature is strongly affected by the surface slope and its orientation [52], [53], the cold T_B is largely correlated with the low FTA values. For example, in Tycho crater, the relatively lower T_B in the northern floor is corresponding to the lower FTA here. Similar phenomenon also occurs in Aristarchus crater. Particularly, at 3.0 GHz maps, the areas of the cold T_B anomaly at noon are much more than those of the crater ranges in Copernicus and Jackson, and they largely agree with the relatively lower FTA distributions. This hints that the FTA should be the dominant factor for the cold anomaly in the four craters.

Table III is the correlation coefficients between the T_B and FTA. But Table III indicates a more complex influence of the FTA on the T_B compared with the RA influence. Here, no regularity can be deduced from Table III, indicating that the correlation between the FTA and the T_B is likely rather weak. Interestingly, the correlation coefficients in Copernicus crater should be paid great attention, where the coefficient is up to 0.96 at 3.0 GHz at noon and they are fairly high even at midnight. Such high coefficients obviously verify that the FTA is likely responsible for the low T_B behaviors over the Moon surface.

Lucey *et al.* also indicated that there may exist the calibration problem for the regions with complex topography when retrieving the FTA using the UV-VIS data [18]. Also, the materials in the depth penetrated by visible signal are easily contaminated by the spacing and ejecta from other place [11], [12], [30]. Therefore, the excellent coincidence between the FTA distribution and the low T_B performance in Copernicus crater can represent the influence to some extent.

Therefore, the low T_B anomaly is likely caused by the low FTA. Additionally, the low T_B anomaly occurs in the four typical craters, indicating that the shallow lunar crust is likely dominated by the materials with very low FTA.

The low FTA can well interpret the low T_B at noon using the theoretical method [14], [27], [32], [54], [55]. However, the low FTA cannot support the low T_B at midnight, which should be high according to the theoretical simulation [14], [27], [32], [54], [55]. Thus, combined with the previous analysis, one more cause for the cold T_B anomaly is the low substrate temperature according to the theoretical model [14], [27], [32], [54], [55].

The existence of the cold anomaly in the crater floors indicates that this is a T_B stable place over the lunar surface. Thereafter, associated with the hour-angle method, the 24-h T_B values in

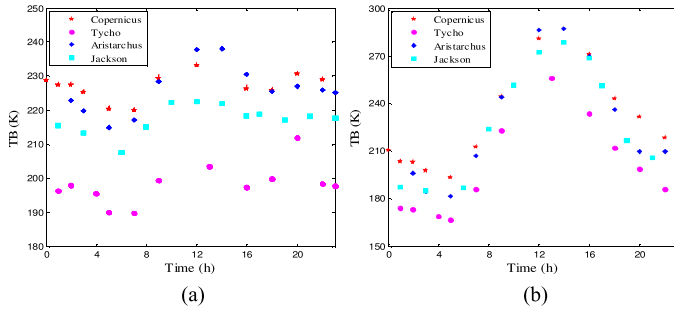


Fig. 9. Diurnal T_B variation within cold anomaly.

the cold T_B anomaly places were extracted and plotted in Fig. 9. It indicates that the changes of T_B with time are stronger at 37.0 GHz than those at 3.0 GHz. This coincides well with the observations described by Hagfors [11], indicating the rationality of the generated T_B curves.

Moreover, the change of T_B at 3.0 GHz is only about 10 K during the whole day, which is about 100 K at 37.0 GHz and more than 200 K in the surface layer with the thermal conduction model [52], [53]. According to the thermal conduction model [14], [22], [28], the physical temperature in the depth layer penetrated by 3.0 GHz microwave is stable in the cold anomaly. In this depth, the physical temperature is dominated by the thermal flux from the interior of the Moon. Therefore, combined with the low FTA in the cold anomalies, the T_B performance at 3.0 GHz at least indicates that the shallow lunar crust is fairly cold. Additionally, the low T_B at noon also means that the temperature in the shallow lunar crust is likely much cooler than that measured during the Apollo missions. This new finding is essentially important to improve understand the thermal history of the Moon.

C. New Perspective of Shallow Lunar Crust

Figs. 3–6 show a new perspective about the upper layer of the lunar regolith. First, the T_B distributions in Figs. 3–6 are much different from the visible features presented in Fig. 1 and the TIR results revealed by Bandfield *et al.* [16], [17], indicating the difference of the regolith thermophysical features in depth compared to the superficial layer. Second, the T_B behaviors are also changed with frequency, hinting the variation of regolith thermophysical features with depth.

Particularly, in Copernicus and Jackson craters, the regions with rather low T_B considerably decrease with frequency. In Copernicus crater, such area is from about 8830 km^2 at 3.0 GHz to nearly 0 at 37.0 GHz at noon and from about 3800 km^2 at 3.0 GHz to about 1650 km^2 at 37.0 GHz at midnight. In Jackson crater, such area is from about 6830 km^2 at 3.0 GHz to only a small patch in the south at 37.0 GHz at noon and from about 5320 km^2 at 3.0 GHz to about 3090 km^2 at 37.0 GHz at midnight. But in Aristarchus, the regions with low T_B only slightly decrease with frequency. Especially in the crater floor, the area of the regions with rather low T_B is almost constant. What is more, in Tycho crater, the area of the regions with low T_B obviously increases with frequency at midnight, which is

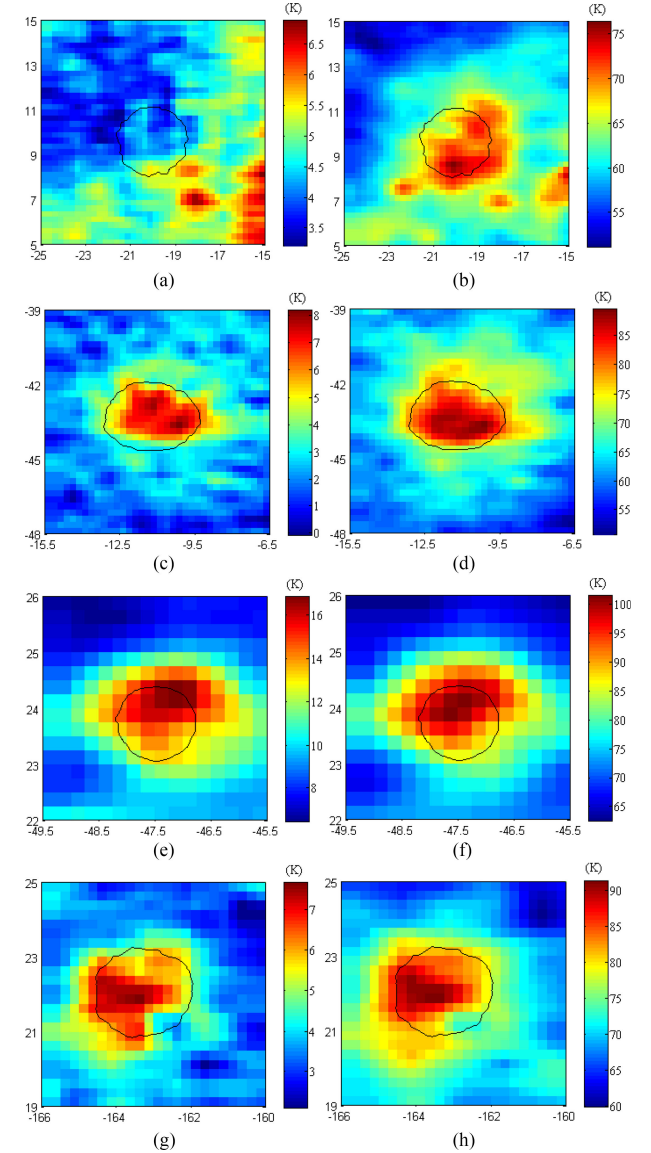


Fig. 10. dT_B maps of four Copernican craters.

from about 260 km^2 at 3.0 GHz to 3780 km^2 at 37.0 GHz. This indicates that the change of the regolith thermophysical features with depth is special for different craters.

Meng *et al.* suggested that the difference between the T_B at noon and dawn at the same frequency, named dT_B , can eliminate the influence of the surface environment, which is directly related to the thermophysical features of the substrate regolith [14], [29]. Thus, the dT_B map is also introduced in this study (see Fig. 10).

Fig. 10 presents another perspective about the Copernican craters. In Copernicus crater, no crater shape can be identified at 3.0 GHz, while the shape of the region with relatively higher dT_B is not severely correlated with the crater. In Tycho crater, the shape of the crater is apparently elongated along the northwest direction. In Aristarchus crater, the regions with high dT_B is elongated in east-west direction but shortened in north-south direction. In Jackson crater, the regions with high dT_B are largely centered in the western part of the crater.

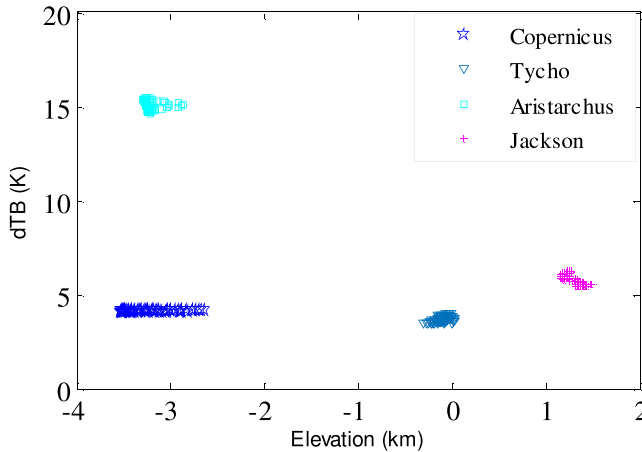


Fig. 11. dT_B at 3.0 GHz in crater floors and the corresponding elevation.

That is, the regions with relatively higher dT_B do not coincide with the crater shape in these craters. Meaningfully, the relatively higher dT_B always occurs in the crater floor. With the distance away from the crater center, the dT_B becomes gradually lower. Especially, in Fig. 10(c) and (g), the dT_B in far distance is less than 3 K at 3.0 GHz.

Additionally, the high dT_B means the large fluctuation of the T_B through a whole day, which is directly resulted from the rather low thermal inertia of the volume lunar regolith [16], [21], [45], [50]. Combined with the size of the craters, the highest dT_B means a material with very low thermal inertia in the crater floor. Also, in the surface layer represented by the lunar regolith far away from the crater center, the small dT_B values hint a comparatively higher thermal inertia than those in the crater floors. Therefore, the difference of the materials in thermal inertia from the crater floor to far distance brings about a new constraint for the cratering formation mechanism.

Moreover, Tycho and Jackson craters are located in the highlands. The fluctuation of the dT_B is rather small in far distance, almost less than 4 K. The similar dT_B performances imply the homogeneity of the lunar regolith. Thus, combined with the cratering mechanism, this means the homogeneity of the shallow lunar regolith. To further understand the thermophysical features of the shallow lunar crust, the dT_B values in crater floors and the corresponding elevations are extracted and plotted in Fig. 11. Although the elevation and latitude position of the crater floors differ greatly from each other, the dT_B values in Copernicus, Tycho, and Jackson craters are nearly identical, which is about 5.0 K. This again hints that the shallow lunar crust is likely homogeneous in thermophysical features.

However, in Copernicus crater, the dT_B behaviors are special compared to others, which presents a low dT_B in the northwest part of the region at 3.0 GHz. Combined with the MTE performances in Mare Imbrium [31], this indicates that the impact ejecta of the crater is in the northwest direction. Also, the ejecta is homogeneous and the thickness is more than that can be penetrated by 3.0 GHz microwave, about 2 m.

In Aristarchus crater floor, the dT_B , about 15 K, is more than 3 times as that in other three craters, though they should have the similar regolith compositions. Aristarchus crater is located

in the southern part of Aristarchus Plateau, which is covered by a thick layer of pyroclastic deposits. The abnormal dT_B features in this crater may give some important information about the deposits here, which deserves to be further studied in future.

At last, the low thermal inertia in the crater floors agrees well with the observed very low T_B at midnight and fairly high dT_B for the poor thermal storage capability of the lunar regolith [20], [21]. However, the low thermal inertia is opposite to the low T_B at noon. Combined with the microwave radiative transfer simulation of the lunar regolith [20], [21], this low T_B at noon is likely brought by the low substrate temperature. Combined the size of the typical Copernican craters and its excavation depth, this again directly implies a low physical temperature of the shallow lunar crust.

V. CONCLUSION

The Copernican craters penetrated the Moon surface to several kilometers, whose MTE could indirectly reflect the thermal physical features and the thermal state of the shallow lunar crust. In this paper, the MTE features of the four typical Copernican craters, including Copernicus, Aristarchus, Tycho, and Jackson, are evaluated using the CELMS data from CE-2 satellite. Several important results are presented as follows.

- 1) The causes to the hot anomaly are reunderstood according to the T_B performances at noon and midnight. Though the RA is important to the anomaly according to the theoretical model, it is not the decisive factor because of the difference between the RA distribution and the corresponding T_B performances. Also, the surface slope and its orientation play an important role in the hot T_B anomaly in Tycho crater, but there does not exist the hot anomaly in Aristarchus and Jackson craters at night, indicating the topography is not the cause for the hot T_B anomaly. Thus, the causes to the hot T_B anomaly are still in doubt, which should be further studied with more sources of the data, and even the *in situ* measurements.
- 2) The cold T_B anomaly is likely brought by the special low-FTA materials. Additionally, the daily variation of the T_B in the cold anomaly is fairly small. This not only hints that the physical temperature in the substrate layer is stable, but also implies a cold state of the shallow lunar crust.
- 3) The T_B performances over the crater floors and the far distance indicate that the thermal inertia of the materials is low in shallow lunar crust. Also, the dT_B performances in the regions far from the crater centers and those in the floors of Copernicus, Tycho, and Jackson craters indicate that the shallow lunar crust is homogeneous in the thermophysical features.

Additionally, the difference of the dT_B from the crater floor to the far distance means the change of the materials in thermal inertia, which will provide a new constraint for the cratering formation mechanism. But, for the short period and low spatial resolution of the CE-1/2 CELMS observations, only limited number of Copernican craters can be identified. More CELMS observations with better spatial resolutions are indispensable in future lunar exploration.

ACKNOWLEDGMENT

The authors would like to thank the reviewers for their valuable and insightful comments. The FTA and RA data were downloaded from JMARS SOFTWARE (<http://oss.mars.asu.edu/svn/jmars/>). The authors are grateful for being allowed to use their data. The authors would also like to thank D. Xiaowei of Jilin University for his work on the preliminary data processing.

REFERENCES

- [1] E. Stöffler and G. Ryder, "Stratigraphy and Isotope ages of lunar geologic units: Chronological standard for the inner solar system," *Space Sci. Rev.*, vol. 96, no. 1–4, pp. 9–54, 2001.
- [2] R. Bugiolacchi *et al.*, "An in-depth look at the lunar crater copernicus: Exposed mineralogy by high-resolution near-infrared spectroscopy," *Icarus*, vol. 213, no. 1, pp. 43–63, 2011.
- [3] H. Hiesinger *et al.*, "Ages and stratigraphy of mare basalts in Oceanus procellarum, mare nubium, mare cognitum, and mare insularum," *J. Geophys. Res. Planets*, vol. 108, no. 1, pp. 1.1–1.27, 2003.
- [4] M. J. Cintala and R. A. F. Grieve, "Scaling impact melting and crater dimensions: Implications for the lunar cratering record," *Meteorit. Planet. Sci.*, vol. 33, no. 6, pp. 889–912, 1998.
- [5] Z. Yue *et al.*, "Projectile remnants in central peaks of lunar impact craters," in *Proc. AGU Fall Meeting, AGU Fall Meeting Abstracts*, pp. 435–437, 2003.
- [6] R. W. K. Potter *et al.*, "Constraining the size of the south pole-aiken basin impact," *Icarus*, vol. 220, no. 2, pp. 730–743, 2012.
- [7] J. D. Stopar *et al.*, "Relative depths of simple craters and the nature of the lunar regolith," *Icarus*, vol. 298, pp. 34–38, 2015.
- [8] G. P. Hu *et al.*, "A rock model for the cold and hot spots in the Chang'E microwave brightness temperature map," *IEEE Trans. Geosci. Remote Sens.*, vol. 56, no. 9, pp. 5471–5480, Sep. 2018.
- [9] Y. C. Zheng *et al.*, "First microwave map of the moon with chang'E-1 data: The role of local time in global imaging," *Icarus*, vol. 219, no. 1, pp. 194–210, 2012.
- [10] T. W. Thompson *et al.*, "A comparison of infrared, radar, and geologic mapping of lunar craters," *Moon*, vol. 10, no. 1, pp. 87–117, 1974.
- [11] T. Hagfors, "Remote probing of the moon by infrared and microwave emissions and by radar," *Radio Sci.*, vol. 5, no. 2, pp. 189–227, 1970.
- [12] G. H. Heiken, D. T. Vaniman, and B. M. French, *A User's Guide to the Moon*. London, U.K.: Cambridge Univ. Press, 1991.
- [13] K. L. Chan *et al.*, "Lunar regolith thermal behavior revealed by Chang'E-1 microwave brightness temperature data," *Earth Planet Sci. Lett.*, vol. 295, no. 1/2, pp. 287–291, 2010.
- [14] Z. G. Meng *et al.*, "Microwave thermal emission at tycho area and its geological significance," *IEEE J. Sel. Topics Appl. Earth Observ. Remote Sens.*, vol. 10, no. 6, pp. 7616–7619, Jun. 2017.
- [15] B. A. Campbell *et al.*, "Focused 70-cm wavelength radar mapping of the Moon," *IEEE Trans. Geosci. Remote Sens.*, vol. 45, pp. 4032–4042, 2007.
- [16] J. L. Bandfield *et al.*, "Lunar surface rock abundance and regolith fines temperatures derived from LRO diviner radiometer data," *J. Geophys. Res. Planets*, vol. 116, no. E12, pp. 1–18, 2011, Art. no. E00H02.
- [17] J. L. Bandfield *et al.*, "Lunar cold spots: Granular flow features and extensive insulating materials surrounding young craters," *Icarus*, vol. 231, no. 4, pp. 221–231, 2014.
- [18] P. G. Lucey, D. T. Blewett, and B. L. Jolliff, "Lunar iron and titanium abundance algorithms based on final processing of Clementine ultraviolet-visible images," *J. Geophys. Res. Planets*, vol. 105, no. E8, pp. 20297–20306, 2000.
- [19] J. J. Gillis, B. L. Jolliff, and R. L. Korotev, "Lunar surface geochemistry: Global concentrations of Th, K, and FeO as derived from lunar prospector and clementine data," *Geochim. Cosmochim. Acta.*, vol. 68, no. 18, pp. 3791–3805, 2004.
- [20] J. M. Saari, R. W. Shorthill, and T. K. Deaton, "Infrared and visible images of the eclipsed moon of December 19, 1964," *Icarus*, vol. 5, no. 1–6, pp. 635–659, 1966.
- [21] W. M. Sinton, "Eclipse temperatures of the lunar crater tycho," in *Proc. Int. Astron. Union*, 1962, vol. 14, pp. 469–471.
- [22] J. S. Jiang and Y. Q. Jin, *Selected Paper on Microwave Exploration of Lunar Surface in Chinese Chang'E-1 Project*. Beijing: Science Press, 2011.
- [23] S. J. Keihm, "Effects of subsurface volume scattering on the lunar microwave brightness temperature spectrum," *Icarus*, vol. 52, no. 3, pp. 570–584, 1982.
- [24] X. H. Gong and Y. Q. Jin, "Diurnal change of thermal emission with 'hot spots' and 'cold spots' of fresh lunar craters observed by Chinese Chang'E-1," *Sci. China Inform. Sci.*, no. 8, pp. 923–935, 2012.
- [25] Z. G. Meng *et al.*, "Potential geological significations of crism basin revealed by CE-2 CELMS data," *ISPRS*, vol. XLII-3, pp. 1279–1284, 2018.
- [26] Z. C. Cai and T. Lan, "Lunar brightness temperature model based on the microwave radiometer data of Chang'E-2," *IEEE Trans. Geosci. Remote Sens.*, vol. 55, no. 10, pp. 5944–5955, Oct. 2017.
- [27] Z. Z. Wang *et al.*, "Lunar surface dielectric constant, regolith thickness, and ^3He abundance distributions retrieved from the microwave brightness temperatures of CE-1 lunar microwave sounder," *Sci. China Earth Sci.*, vol. 53, no. 9, pp. 1365–1378, 2010.
- [28] T. Fang and W. Z. Fa, "High frequency thermal emission from the lunar surface and near surface temperature of the Moon from Chang'E-2 microwave radiometer," *Icarus*, vol. 232, pp. 34–53, 2014.
- [29] Z. G. Meng *et al.*, "Microwave thermal emission features of mare orientale revealed by CELMS data," *IEEE J. Sel. Topics Appl. Earth Observ. Remote Sens.*, vol. 10, no. 6, pp. 2991–2998, Jun. 2017.
- [30] D. F. Winter, "Infrared emission from the surface of the moon," *Adv. Astron. Astrophys.*, vol. 9, pp. 203–243, 1972.
- [31] Z. G. Meng *et al.*, "Passive microwave probing mare basalts in mare imbrrium using CE-2 CELMS data," *IEEE J. Sel. Topics Appl. Earth Observ. Remote Sens.*, vol. 11, no. 9, pp. 3097–3104, Sep. 2018.
- [32] Z. G. Meng *et al.*, "Influence of $(\text{FeO} + \text{TiO}_2)$ abundance on the microwave thermal emissions of lunar regolith," *Sci. China Earth Sci.*, vol. 59, no. 7, pp. 1498–1507, 2016.
- [33] L. He *et al.*, "Effect of surface roughness on microwave brightness temperature from lunar surface: Numerical analysis with a hybrid method," *Adv. Space Res.*, vol. 51, no. 1, pp. 179–187, 2013.
- [34] C. M. Pieters, "Copernicus crater central peak: Lunar mountain of unique composition," *Science*, vol. 215, no. 4528, pp. 59–61, 1982.
- [35] C. M. Pieters and D. E. Wilhelms, "Origin of olivine at copernicus," *J. Geophys. Res.-Sol. EA.*, vol. 90, no. S02, pp. C415–C420, 1985.
- [36] S. Smrekar and C. M. Pieters, "Near-infrared spectroscopy of probable impact melt from three large lunar highland craters," *Icarus*, vol. 63, no. 3, pp. 442–452, 1985.
- [37] D. Dhingra *et al.*, "Compositional diversity at theophilus crater: Understanding the geological context of Mg-spinel bearing central peaks," *Geophys. Res. Lett.*, vol. 38, no. 11, pp. 467–475, 2011.
- [38] T. Arai *et al.*, "Possible crustal boundary exposed at lunar copernicus crater," in *Proc. Lunar Planetary Sci. Conf.*, vol. 42, 2011, p. 2139.
- [39] G. P. Hu *et al.*, "Qualitative verification of CE-2's microwave measurement: Relative calibration based on brightness temperature model and data fusion," *IEEE Trans. Geosci. Remote Sens.*, vol. 54, no. 3, pp. 1598–1609, Mar. 2016.
- [40] K. A. Howard and H. G. Wilshire, "Flows of impact melt at lunar craters," *Res. US Geol. Surv.*, vol. 3, no. 2, pp. 237–251, 1975.
- [41] B. R. Hawke and J. W. Head, "Impact melt on lunar crater rims," *Impact and Explosion Cratering*, Pergamon Press, New York, pp. 815–841, 1977.
- [42] D. Dhingra, J. W. Head, and C. M. Pieters, "Geological mapping of impact melt deposits at lunar complex craters jackson and tycho: Morphologic and topographic diversity and relation to the cratering process," *Icarus*, vol. 283, pp. 368–381, 2016.
- [43] L. M. Carter *et al.*, "Initial observations of lunar impact melts and ejecta flows with the Mini-RF radar," *J. Geophys. Res. Planets*, vol. 117, no. E00H09, pp. 1–13, 2012.
- [44] S. D. Price, D. Mizuno, and T. L. Murdoch, "Thermal profiles of the eclipsed moon," *Adv. Space. Res.*, vol. 31, no. 11, pp. 2299–2304, 2003.
- [45] J. W. Salisbury and G. R. Hunt, "Infrared images of tycho on dark moon," *Science*, vol. 155, no. 3766, pp. 1098–1100, 1967.
- [46] A. S. McEwen *et al.*, "Clementine observations of the aristarchus region of the moon," *Science*, vol. 266, no. 5192, pp. 1858–1862, 1994.
- [47] S. L. Mouélic *et al.*, "Discrimination between maturity and composition of lunar soils from integrated clementine UV-visible/near-infrared data: Application to the aristarchus plateau," *J. Geophys. Res.*, vol. 105, no. E4, pp. 9445–9455, 2000.
- [48] M. Ohtake *et al.*, "The global distribution of pure anorthosite on the Moon," *Nature*, vol. 461, no. 7261, pp. 236–240, 2009.
- [49] B. L. Jolliff *et al.*, "Major lunar crustal terranes: Surface expressions and crust-mantle origins," *J. Geophys. Res. Planets*, vol. 105, no. E2, pp. 4197–4216, 2000.

- [50] B. C. Murray and R. L. Wildey, "Surface temperature variations during the lunar nighttime," *Astrophys. J.*, vol. 139, no. 5, pp. 734–750, 1964.
- [51] J. P. Williams *et al.*, "The global surface temperatures of the moon as measured by the diviner lunar radiometer experiment," *Icarus*, vol. 283, pp. 300–325, 2017.
- [52] Z. G. Meng *et al.*, "Influence of lunar topography on simulated surface temperature," *Adv. Space Res.*, vol. 54, pp. 2131–2139, 2014.
- [53] G. P. Hu *et al.*, "Brightness temperature calculation of lunar crater: Interpretation of topographic effect on microwave data from Chang'e," *IEEE Trans. Geosci. Remote Sens.*, vol. 52, no. 8, pp. 4499–4510, Aug. 2014.
- [54] Y. Q. Jin, F. H. Yan, and Z. C. Liang, "Simulation for remote sensing of the lunar soil and rock by using multi-channels microwave radiometers," *Chin. J. Radio Sci.*, vol. 18, pp. 477–486, 2003.
- [55] W. Z. Fa and Y. Q. Jin, "Quantitative estimation of helium-3 spatial distribution in the lunar regolith layer," *Icarus*, vol. 71, pp. 15–23, 2007.



Zhiguo Meng (M'16) received the Ph.D. degree in geophysics from Jilin University, Changchun, China, in 2008.

He is currently a Professor in the College of Geo-exploration Science and Technology, Jilin University. His research interests include the application and development of microwave remote sensing technology in the planetary science, primarily the microwave measurement of the lunar regolith.



Xiangyue Li is currently working toward the master's degree with the College of Geoexploration Science and Technology at Jilin University, Changchun, China.

Her research interests include lunar surface temperature simulation and application of the Chang'E Lunar Microwave Sounder data.



Shengbo Chen received the Ph.D. degree in earth exploration and information technology from Jilin University, Changchun, China, in 2000.

He is currently a Professor in the College of Geoexploration Science and Technology, Jilin University. His current research interests include information mechanism of remote sensing, inversion of land surface physical parameters, lunar and planetary remote sensing, the processing methods of remote sensing data, inversion of earth and lunar surface rock mineral composition based on hyperspectral remote

sensing, and the research on technology and method based on comprehensive application of remote sensing, Beidou and communication satellites. He has published more than 200 scientific papers.



Yongchun Zheng received the Ph.D. degree in geochemistry from the University of Chinese Academy of Sciences, Beijing, China, in 2005.

He is currently a Researcher with the National Astronomical Observatories, Chinese Academy of Sciences. His research interests include the study of lunar and planetary geology, the understanding of the Moon and Mars regolith, the utilization of planetary resources, the surface environment of planet, and the scientific goals and future development strategies of the Moon and deep space exploration.



Jiancheng Shi (M'95–SM'02–F'14) received the Ph.D. degree in geography from the University of California, Santa Barbara (UCSB), Santa Barbara, CA, USA, in 1991.

He joined the Institute for Computational Earth System Sciences, UCSB, as a Research Professor. He has worked as a PI for more than ten research projects for NASA, EAS, and JAXA. He has authored more than 300 papers in journals and conferences. In 2010, he became the Director and Senior Research Scientist with the State Key Laboratory of Remote Sensing Science, Institute of Remote Sensing and Digital Earth, Chinese Academy of Sciences. He is currently the PI of the Water Cycle Observation Mission (WCOM). His research interests include microwave remote sensing of water cycle-related components and data assimilation.

Dr. Shi is a Fellow of the Electromagnetics Academy, IEEE and SPIE.



Tianxing Wang (M'12) received the Ph.D. degree in GIS/remote sensing from Beijing Normal University, Beijing, China, in 2011.

He is currently an Associated Researcher in the State Key Laboratory of Remote Sensing Science, Institute of Remote Sensing and Digital Earth, Chinese Academy of Sciences. His research interests focus on retrieval of land surface biophysical parameters from satellite data, land surface radiation budget over rugged terrain for all-sky conditions, atmospheric CO₂ monitoring, hyperspectral data processing, and remote sensing applications related to climate change.



Yuanzhi Zhang (S'99–A'03–M'05) received the Doctor of Science degree in technology from Helsinki University of Technology, Finland, in 2005.

He joined the Chinese University of Hong Kong in 2006 and the University of Chinese Academy of Sciences in 2014. He is currently a Researcher with the National Astronomical Observatories, Chinese Academy of Sciences. His research interests include coastal zone studies, land use and land cover change detection, water quality monitoring, urban heat island effect, geothermal resource, and lunar and deep-space

exploration using remote sensing data.



Jinsong Ping received the Ph.D. degree in astronomy from Shanghai Astronomical Observatory, Chinese Academy of Sciences, Shanghai, China, in 1996.

He is currently a Researcher in National Astronomical Observatories, Chinese Academy of Sciences, Beijing, China. His research interests include physics and dynamics for moons and planets, radio astrometry, and modeling the ionospheres for the earth and Mars with earth-based data.

Dr. Ping is a Member of Division A Fundamental Astronomy, Division B Facilities, Technologies and Data Science, Division E Sun and Heliosphere, Division F Planetary Systems and Bioastronomy, and Inter-Division A-F WG Cartographic Coordinates & Rotational Elements.



Yu Lu is currently working toward the master's degree with the School of Geography and Ocean Science at Nanjing University, Nanjing, China.

His research interests include planetary remote sensing.